

Structural, magnetic, electric and electronic aspects of the $\text{Ba}_2\text{YbSbO}_6$ perovskite material

L.A. Carrero Bermúdez, R. Moreno Mendoza, R. Cardona,
D.A. Landínez Téllez, J. Roa-Rojas*

Grupo de Física de Nuevos Materiales, Departamento de
Física, Universidad Nacional de Colombia, A.A. 5997, Bogotá DC, Colombia
) Email: jroar@unal.edu.co



Received 19 June 2017; Accepted 22 Aug. 2017; Accepted 15 Sep. 2017

A single crystallographic phase of the $\text{Ba}_2\text{YbSbO}_6$ perovskite was synthesized by the solid-state reaction method. From the refinement of the XRD pattern it was obtained that this sintered material crystallizes in a rhombohedral complex perovskite, R-3 (#148) space group. SEM images showed the sub-micrometric character of its granular surface. Measurements of susceptibility as a function of temperature evidenced the antiferromagnetic behavior of this material below the Néel temperature $T_N=118$ K and a paramagnetic feature above this critical temperature. The magnetic parameters were obtained from the fitting of susceptibility in the paramagnetic regime with the Curie-Weiss equation. From theoretically calculated Density of States and band structure the semiconductor characteristic of the material was determined and the energy gap was predicted for the up and down spin orientations of the electron gas close to the Fermi level. The energy gap value was experimentally corroborated from diffuse reflectance spectra with the Kubelka-Munk fit of the experimental result. Measurements of dielectric constant as a function of applied frequencies at room temperature reveal a decreasing behavior.

Keywords: Perovskite; Characterization; Electronic structure.

1. INTRODUCTION

In the last years the complex perovskites with generic formula $\text{A}_2\text{BB}'\text{O}_6$ [1-3] have been subject of enhanced scientific studies because the wide range of applications that these materials present on an industrial scale. Double perovskites belonging to the series $\text{Ba}_2\text{LnB}'\text{O}_6$ ($\text{Ln}=\text{lanthanide}$ and Y^{3+} and $\text{B}'=\text{Nb}^{5+}$, Ta^{5+} , Sb^{5+}) are of interest due to their potential use as substrates for high- T_c superconductors [4,5] and their likely high chemical compatibility with the structurally analogous, oxygen deficient double perovskites, $\text{Ba}_2\text{LnSnO}_6$, which is a series of interest for use as solid-state electrolytes due to their high ionic conductivity [6,7]. Substitution of Nb^{5+} , Ta^{5+} , Sb^{5+} could provide a method of controlling the oxygen stoichiometry of these compounds, potentially minimizing the problems caused by reduction of $\text{Ba}_2\text{LnSnO}_6$ that is thought to be a consequence of the large level of oxygen vacancies in

these compounds [6]. Phase transitions in perovskites have long been of interest to solid-state chemists [8]. Previous studies [9, 10], using laboratory X-ray and medium resolution neutron diffraction, reported that the structures in the series $\text{Ba}_2\text{LnSbO}_6$ change from $R\bar{3}$ rhombohedral (tilt system $a^-a^-a^-$) to $Fm\bar{3}m$ cubic ($a^0a^0a^0$) symmetry with decreasing size of the Ln^{3+} cation. That the symmetry increases as the ionic radius of the lanthanide decreases, this is consistent with the increase of the tolerance factor, which in double perovskites is given by $\tau = \frac{r_A+r_O}{\sqrt{2}\left(\frac{r_B+r_{B'}}{2}+r_O\right)}$, where r_A , r_B , $r_{B'}$ and r_O are the ionic radii of the A , B , B' , and O ions, respectively [11]. An increase in the tolerance factor indicates that the volume of the BO_6 octahedron is better matched to the size of the AO_{12} polyhedron reducing the need for the octahedral tilting to accommodate this A -site cation. Since octahedral tilting is responsible for the lowering of the symmetry from cubic, the symmetry tends to increase, as the B -type cation gets smaller. The aim of this work is to carry out a detailed *ab initio* theoretical study of the $\text{Ba}_2\text{YbSbO}_6$ material, which belongs to this interesting complex perovskite family, and establish a correlation with experimental results of crystalline structure, electric behavior, magnetic response and energy gap. The understanding of these properties is essential in order to elaborate a comprehensive scheme of the potential application of the rare earth Sb -based double perovskites.

2. EXPERIMENTAL PROCEDURE

The $\text{Ba}_2\text{YbSbO}_6$ samples were produced by the solid-state reaction method, from oxide powders of Yb_2O_3 , Sb_2O_5 and Ba_2CO_3 (Aldrich 99.9%), which were stoichiometrically mixed according to the chemical formula $\text{Ba}_2\text{YbSbO}_6$. Then, the resultant mixture was grinded and pressed to form a pellet of 9.0 mm diameter and annealed at 1000 °C for 30 h. The samples were then remacerated, repelletized and sintered at 1100 °C for 40 h and 1200 °C for 40 h. The crystalline structure was studied from X-ray diffraction (XRD) by means of a PW1710 diffractometer ($\lambda_{\text{CuK}\alpha}=1.54064 \text{ \AA}$). Rietveld refinement of the experimental data was performed through the GSAS code [12]. Morphological surface studies were carried out by means scanning electron microscopy (SEM) experiments by the utilization of a VEGA 3 electronic microscope. Field cooling measurements of the magnetic susceptibility as a function of temperature were studied by using a MPMS Quantum Design SQUID. Diffuse reflectance experiments were performed by using a VARIAN Cary 5000 UV-Vis-NIR spectrophotometer, which has an integration sphere with a PMT/Pbs detector. The value of the relative dielectric constant was established by using an Agilent HP4194A-350 frequency analyzer.

3. CALCULATION METHOD

The electronic and band structures were predicted from the application of the Full-Potential Linear Augmented Plane Wave method (FP-LAPW) within the framework of the Kohn-Sham Density Functional Theory (DFT) [13]. The exchange and correlation effects were treated by using the Generalized Gradient Approximation (GGA) [14]. This potential considers the difference between the electronic densities for the two distinct spin orientations from the beginning. The self-consistent process was developed by the numeric package Wien2k [13]. Taking the experimental unit cell data as input (with a formula unit), the structure studied in this work were fully relaxed with respect to their lattice parameters and the internal degrees of freedom compatible with the space group symmetry of the crystal structure. The resulting energies versus volume functions have been fitted to the equation of state due to Murnaghan [15] in order to obtain the minimum energy value, the bulk modulus, its pressure derivative and the equilibrium lattice parameters and associated volume. The muffin-tin radii used for

$\text{Ba}_2\text{YbSbO}_6$ were 2.20, 2.50, 2.12 and 1.82 Bohr for Ba, Yb, Sb and O respectively, angular momentum up to $l = 10$ inside the muffin-tin sphere, a maximum vector in the reciprocal space of $G_{\text{max}} = 12.0$. Energy convergence tests were performed and $RMT \cdot K_{\text{max}} = 7.0$ was selected for calculations. A mesh of 1000 points in the first Brillouin zone (equivalent to a maximum of 250 k points in the irreducible Brillouin zone) was used. Finally, the convergence criterion for the self-consistent calculation was 0.0001 Ry for the total energies and 1.0 mRy/u.a. in the internal forces. Spin polarization was included in the calculations.

4. RESULTS AND DISCUSSION

The refined experimental pattern of XRD result for $\text{Ba}_2\text{YbSbO}_6$ is shown in figure 1. The black line represents the experimental data and red line corresponds to the simulated pattern by means of the GSAS code. Base line is the difference between theoretical and experimental results. Refinement parameters of figure 1 were $\chi^2 = 7.613$, $R_{(F2)} = 6.04\%$. The Rietveld refinement permitted to establish that this material adopts a rhombohedral perovskite structure, which belongs to the $R-3$ (#148) space group. The lattice parameter obtained from the refinement is $a = 5,9104 \text{ \AA}$ with trigonal angle $\alpha = 59,9993^\circ$. These results are 99.0% in agreement with the theoretical values obtained from the Structure Prediction Diagnostic Software *SPuDS* [16], which predicts $a = 5,9672 \text{ \AA}$ and $\alpha = 59.6389^\circ$.

The found structure corresponds to the $a-a-a-$ tilt system in the Glazer notation. The crystallization of $\text{Ba}_2\text{YbSbO}_6$ in the $R-3$ (#148) space group can be corroborated taking into account that the XRD pattern corresponding to this symmetry involves reflections, signaling odd-odd-odd reflections, which is characterized by cationic ordering and simple octahedral tilting.

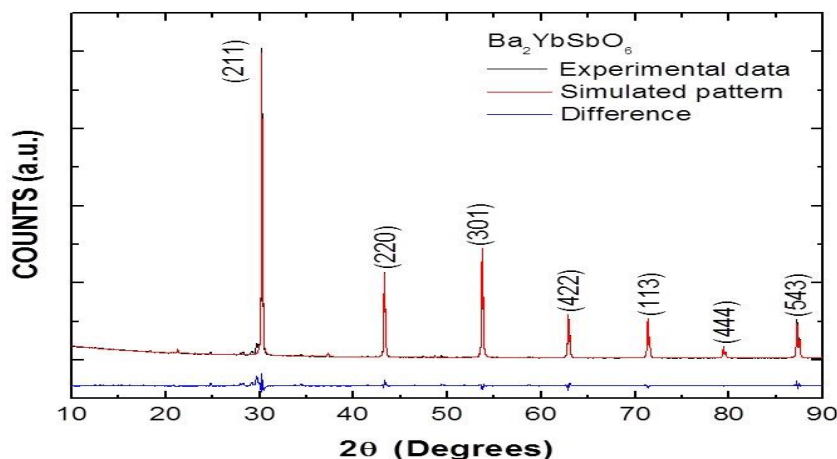


Figure 1 Characteristic XRD pattern for the $\text{Ba}_2\text{YbSbO}_6$ double perovskite. Symbols represent experimental diffraction data; continuous lines are the simulated patterns and base line is the difference between experimental and calculated values.

In the study and description of crystallographic structures the concept of *positions* is fundamental [17]. Then, the so-called Wyckoff positions for this structure were experimentally determined to be $Ba=2c$, $Yb=1a$, $Sb=1b$ and $O=6f$. In this notation, a , b , c and f are the Wyckoff letters that determine all the points x for which the site-symmetry groups are conjugate subgroups of the $R-3$ [18]. These letters constitute just a coding frame for the Wyckoff positions, starting with a at the bottom position and continuing in alphabetical order [17]. The number of equivalent points per unit cell, which accompanies the letter of Wyckoff, is known as multiplicity of the Wyckoff position. In the case of the $R-3$ (#148) space group, the Wyckoff

letter a has a unique possible coordinate $(0,0,0)$ and therefore its multiplicity is 1. In the same way, b has $(\frac{1}{2},\frac{1}{2},\frac{1}{2})$. On the other hand, c has multiplicity 2, because this position may have coordinates (x,x,x) and $(-x,-x,-x)$. For this Wyckoff position we have obtained $(\frac{1}{4},\frac{1}{4},\frac{1}{4})$. At last, f has multiplicity 6, with possible coordinates (x,y,z) ; (z,x,y) ; (y,z,x) ; $(-x,-y,-z)$; $(-z,-x,-y)$ and $(-y,-z,-x)$. In our case the position $(-0.2256, -0.2997, 0.2628)$ was obtained.

The tolerance factor calculated from the experimental data is $\tau=0.9335$, which is in accordance with expected values for the trigonal perovskite structures [16]. From the refinement analysis the octahedral distribution in the structure of the $\text{Ba}_2\text{YbSbO}_6$ material was constructed showed in figure 2. In this figure a marked difference between the orientation of the Yb-O_6 and Sb-O_6 octahedra is perceived. This octahedral disorientation is due to differences in the ionic radii of the cations Yb^{3+} and Sb^{5+} , as well as to the differences between the links of the two cations in their octahedral coordination with the oxygen anions.

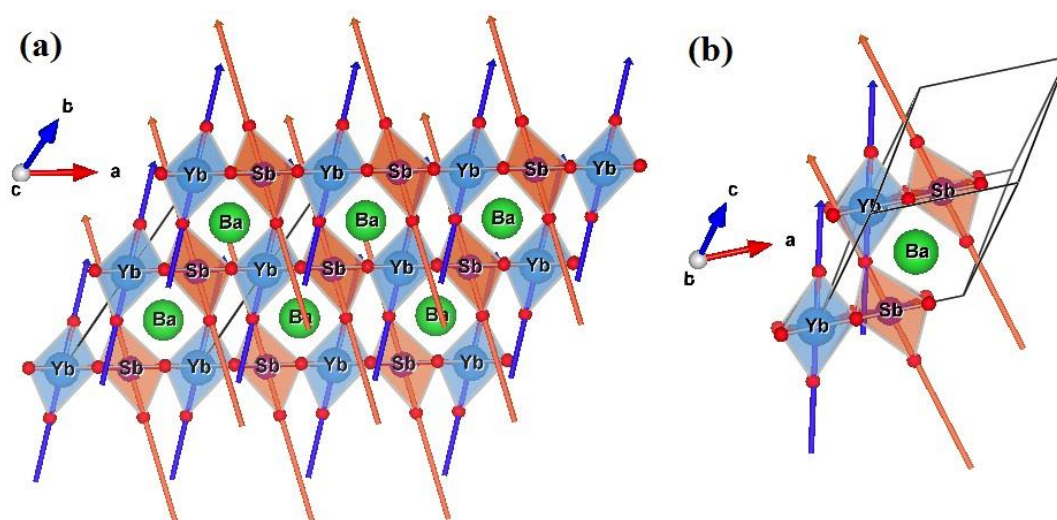


Figure 2 Structure of the $\text{Ba}_2\text{YbSbO}_6$ for the $R-3$ space group in the planes (a) ab and (b) ac .

An important observation about the structural distortion is related to the tilt angle of the octahedra, which is obtained to be $\beta_{\text{Yb}}=17.965^\circ$ for Yb-O_6 and $\beta_{\text{Sb}}=-16.887^\circ$ for Sb-O_6 , for a total deviation of 34.852° between their directions.

SEM image of the material shown in figure 3 reveals a qualitative approximation to the surface microstructure. In picture 3a evidences the formation of clusters of polyhedral grains and interstitial particulate grains. By applying the intercept technique in picture 3b, it is clear that the grains could end up having a few tenths of a micron, form groups, which have appearance of clusters over $2\ \mu\text{m}$.

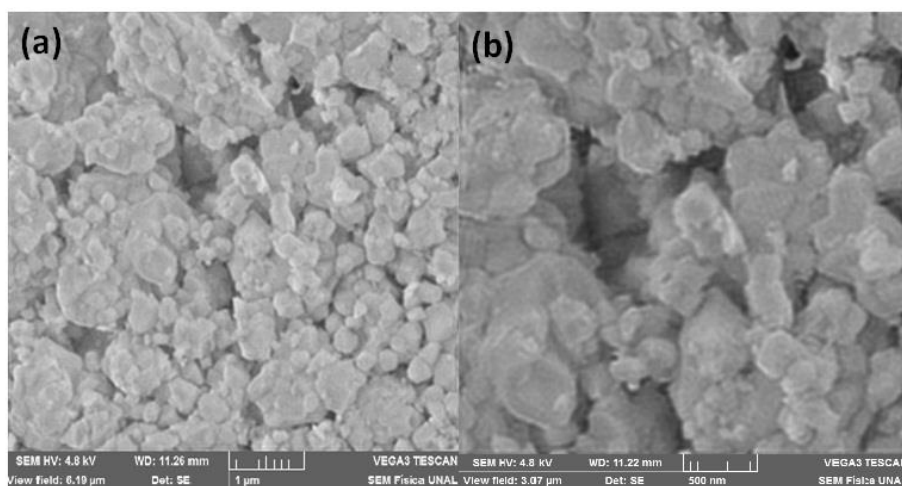


Figure 3 SEM images of Ba₂YbSbO₆ for magnifications (a) 32500x and (b) 65000x.

From measurements of magnetic susceptibility as a function of temperature the magnetic response of the Ba₂YbSbO₆ complex perovskite was examined. As observed in figure 4, the magnetic behavior of this material has a paramagnetic signature at high temperatures.

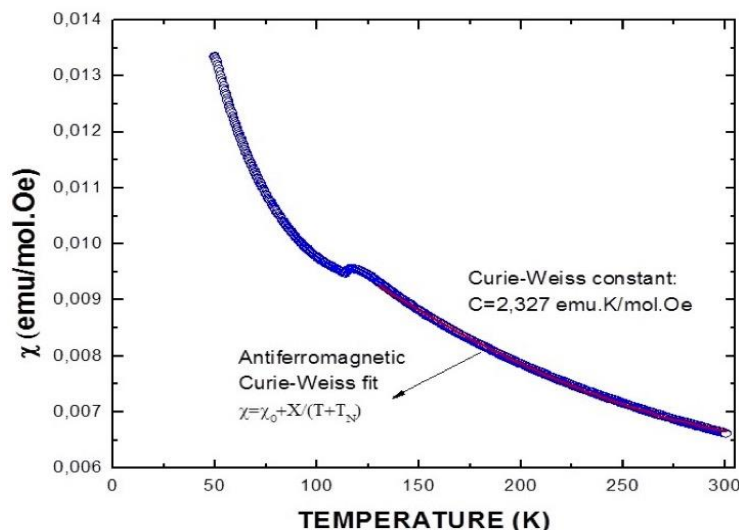


Figure 4 Magnetic susceptibility as a function of temperature measured for the $\text{Ba}_2\text{YbSbO}_6$ material.

Magnetic parameters were obtained from the Curie-Weiss equation $\chi = \chi_0 + \left(\frac{C}{T+T_N}\right)$, where $C = \frac{N\mu_{eff}^2}{3K_B} = 2,327 \text{ emu.K/mol.Oe}$ is the Curie constant, N is Avogadro's number, μ_{eff} is the effective magnetic moment ($\mu_{eff} = P_{eff}\mu_B$), P_{eff} represent the effective Bohr magneton number, μ_B is the Bohr magneton, K_B is the Boltzmann constant and $\chi_0 = 0,00439 \text{ emu/mol.Oe}$ is the temperature independent susceptibility term. From the Curie constant C the effective magnetic moments for $\text{Ba}_2\text{YbSbO}_6$ material was calculated to be $4,31 \mu_B$. This value is 95% in agreement with the theoretical expected moment obtained from the Hund's rules for the Yb^{3+} isolated cation as $g\sqrt{J(J+1)} = 4,54 \mu_B$ [19]. The Néel temperature $T_N = 118 \text{ K}$ was obtained from the Curie-Weiss fitting of the experimental data. We notice that the anomaly observed in figure for $T = 118 \text{ K}$ is directly related with the critical temperature of magnetic ordering.

Because the antiferromagnetic behavior obtained from the fitting of the experimental data to the Curie-Weiss equation, three different antiferromagnetic configurations (AFM1, AFM2 and AFM3) were analyzed in order to study the electronic structure of the Yb and Sb sub-lattices, as shown in figure 5. The minimum energy configuration was obtained by the optimization of the atomic positions and the cell parameter settings for each magnetic configuration, using variable cell relax calculation based on the experimental lattice parameters. Since the AFM1 is the most stable configuration wherein the antiferromagnetic coupling exists between (001) crystallographic planes of $\text{Ba}_2\text{YbSbO}_6$ hereinafter, only this configuration was considered for the density of states calculations.

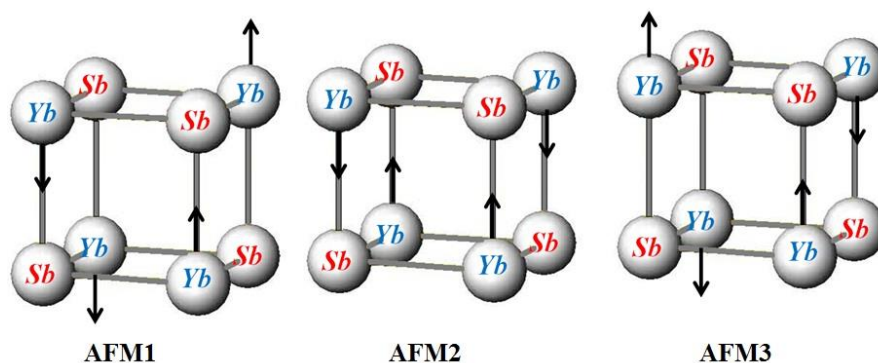


Figure 5 Antiferromagnetic configurations considered for the study of the electronic structure in the $\text{Ba}_2\text{YbSbO}_6$ perovskite material.

Figure 6 shows the band structure (a) and Total Density of States (b) for the $\text{Ba}_2\text{YbSbO}_6$ complex perovskite for both down and up spin polarizations. It is observed in the picture that this material behaves as semiconductor of indirect gap through the Fermi level (energy gap $E_g=2.3 \text{ eV}$) for the spin down polarization and conductor with for the other. It is important to elucidate that the scales are not similar for 6a and 6b pictures. In other words, for the spin down orientation the valence band is majority due to the *Yb* orbital contributions close to the Fermi level. On the other hand, for the up-spin polarization, the valence and conductor band are continuous across the Fermi level but also due to the *Yb* orbital contributions. In the conduction band a set of available states are sited in the energy value 2.25 eV and corresponds to *O* contributions.

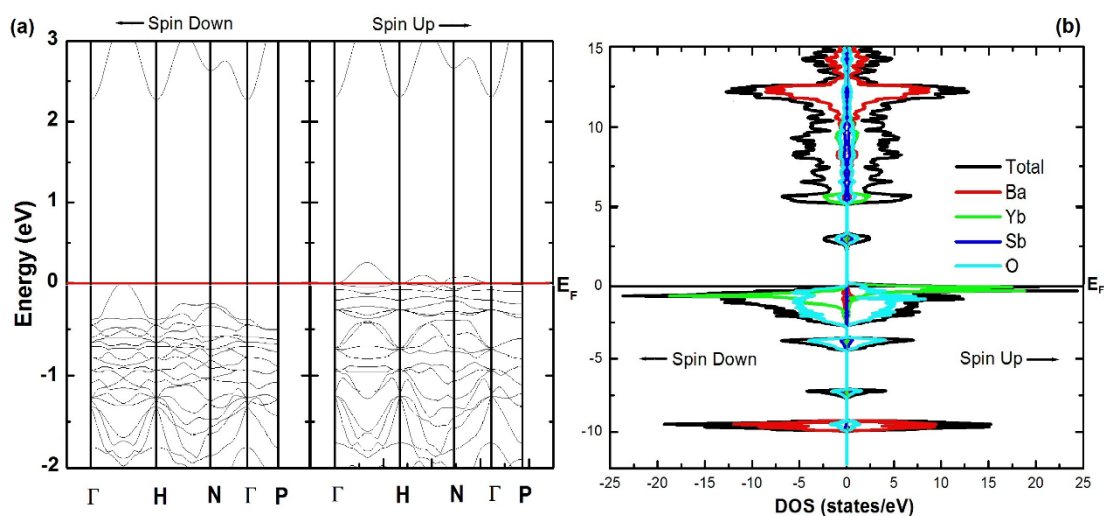


Figure 6 Band structure (a) and Total Density of States (b) for down and up spin polarizations.

Figure 7a exemplifies the partial Density of States calculated for the *Yb*, *Sb*, *Ba* and *O* separate ions. On the other hand, figure 7b exemplifies the contribution of several *Yb* and *O* orbital to the Density of States close the fermi level. From these pictures it is clear that close to the Fermi level the *Yb-4f* orbital are responsible for the conductor behavior for the spin up orientation and the semiconductor character for the spin down polarization. *O-2p* orbital has an incipient contribution in the valence band but a relative contribution in the localized states of the conduction band. Magnetic moment of mixed charge density was calculated from the asymmetry of the *Yb-4f* states close the Fermi level.

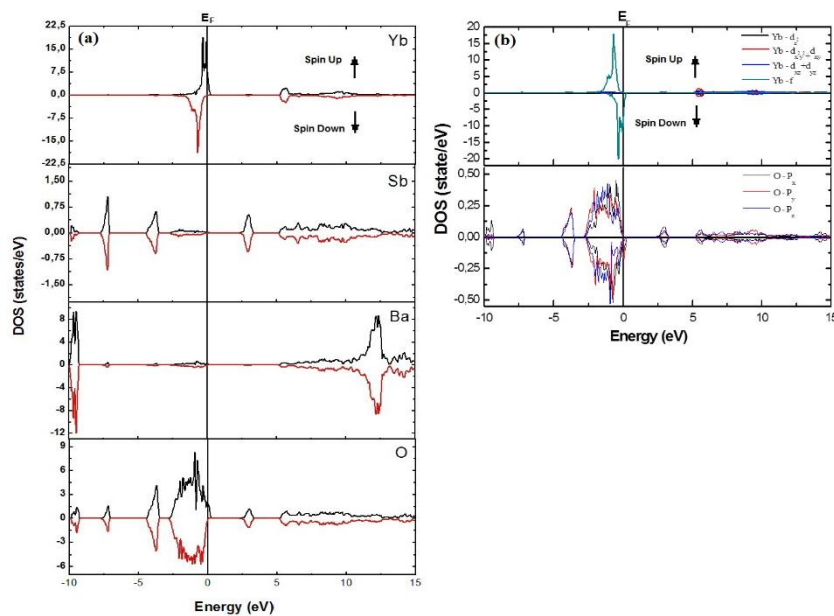


Figure 7 Partial Density of States for (a) the Yb, Sb, Ba and O ions, and (b) Yb and O orbital. Fermi level is identified in $E=0$ eV.

Total magnetic moment in cell was determined to be $5.0 \mu_B$ for Ba_2YbSbO_6 . This result is 14% higher than the experimentally obtained. However, an important element to be taken into account has to do with the clutter of *Yb* and *Sb* cations in the structure of the double perovskite, which can not only distorted octahedra but also modify the magnetic response of the material. The integer theoretical value of the effective magnetic moment and the conductor characteristics of the band structure for the spin up states and semiconductor for the others suggest a tendency of this material to a half-metallic behavior [20].

Results of diffuse reflectance experiments are shown in figure 8a. In the picture, reflectance values experimentally acquired with a step of 1 nm over the $300\text{--}2500 \text{ nm}$ range are schematized. From the absorption of UV-Vis-NIR radiation it was observed that the molecules of the Ba_2YbSbO_6 material cause the weak excitation of electrons from the ground state to excited state. The radiated energy, the quantum characteristics energy dependent from the electronic configuration was calculated. As presented in figure 8b, from the adjustment to the Kubelka–Munk equation the energy gap of the Ba_2YbSbO_6 was determined to be 3.62 eV , which is relatively greater than that predicted by the band structure calculations. DFT calculations predict the Ba_2YbSbO_6 perovskite behaving as a semiconductor with $E_g=2.3 \text{ eV}$ while the diffuse reflectance results suggest a behavior of the material as a weak semiconductor with $E_g=3.62 \text{ eV}$. This difference occurs because in the DFT calculations, the exchange and correlation potential by Perdew, Burke and Ernzerhof [14] gives a very good approximation for the valence and conduction density of states, but is not very accurate for determining the

energy gap in semiconductors due to self-interaction errors [21-22], for which it would be more interesting to use a potential specifically designed for this purpose, that uses local functional without Hartree-Fock exchange [23-24]. Thus, considering the uncertainty inherent in calculating the exact value of the Fermi level, from the results presented in figures 7b (DOS) and 8b (experimental energy gap), it is clear that the material behaves as a semiconductor. Our experimental value of the band gap is comparable with that reported for oxygen-deficient SrTiO₃ ($E_g=3.2$ eV) [25].

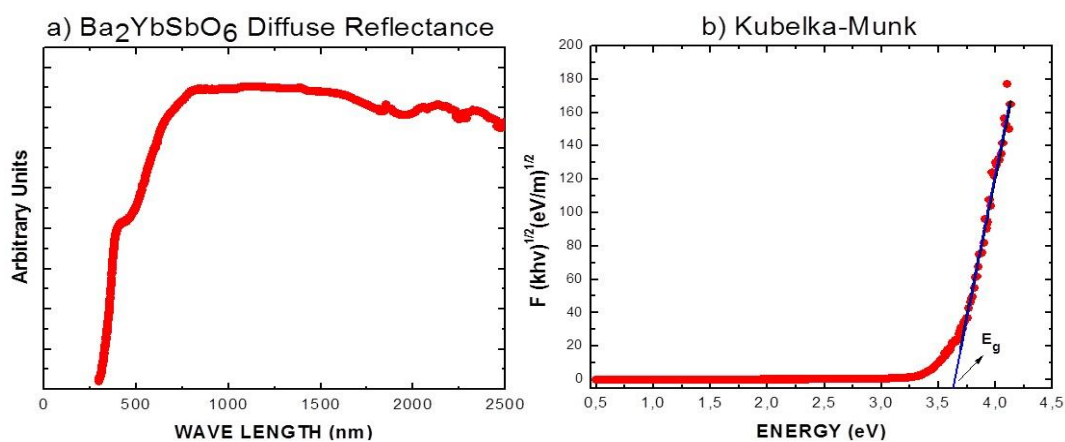


Figure 8 (a) Diffuse reflectance results for the Ba₂YbSbO₆ material. (b) Kubelka–Munk fitting.

In order to elucidate the dielectric characteristics of this compound, measurements of the dielectric constant as a function of frequency performed. The corresponding results are shown in Figure 9. As shown in the drawing, at low frequencies ($\nu=100$ Hz) the value of the dielectric constant $\epsilon=333$, which is very close to the value reported for strontium titanate SrTiO₃ [26]. The value of the dielectric constant decreases dramatically with increasing frequency between 100 Hz and 300 Hz. Above $\nu=400$ Hz, the dielectric constant decreases smoothly to the value $\epsilon=14$ at $\nu=10$ kHz. This result is consistent with reports, according to which, in semiconductor materials the value of the dielectric constant at low frequencies is maximum [27].

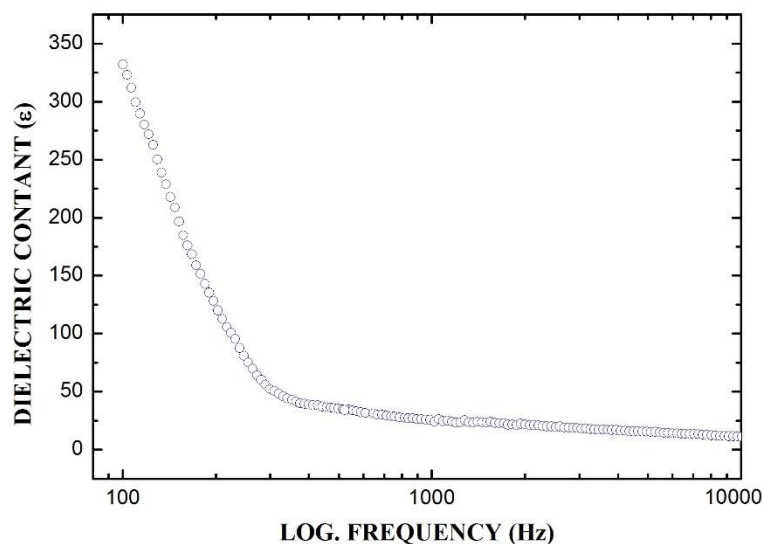


Figure 9 Dielectric constant measured as a function of applied frequency for the $\text{Ba}_2\text{YbSbO}_6$ complex perovskite.

In the *d-band* SrTiO_3 , the feature of large gap semiconductor is due to the broadening of the energy levels of the *Ti-O* octahedron and to the coexistence of free and delocalized excitations. In $\text{Ba}_2\text{YbSbO}_6$ double perovskite there are two types of octahedrons, *Yb-O* and *Sb-O*, but it is clear in figures 6 and 7 that the delocalized states in the valence band are only due to the *d-Sb* orbitals. On the other hand, as observed in the inset of figure 1, there is a noticeable difference between the orientations of the *Yb-O*₆ and *Sb-O*₆ octahedral. This crystallographic feature can substantially modify the energy levels in the *Sb-O*₆ octahedra giving rise to a semiconductor behavior, which is dominant over the apparent conductor nature of the *Yb* spin-up valence electrons.

5. CONCLUSIONS

The synthesis of the $\text{Ba}_2\text{YbSbO}_6$ new material by the solid-state reaction recipe was performed. Characterization of the crystalline structure through the X-ray diffraction technique and Rietveld refinement of the experimental data by using the GSAS code reveal this material crystallizes in a rhombohedral perovskite-like structure with cell parameter $a=5.9104(1)$ Å and tilt angle $\alpha=59.9993(0)^\circ$. Measurements of diffuse reflectance permitted to determine the weak semiconductor character of this material with an energy gap of 3.62 eV. By means experiments of magnetic susceptibility as a function of temperature the paramagnetic response of the $\text{Ba}_2\text{YbSbO}_6$ was analyzed. The fit to the Curie equation gives an effective magnetic moment of $4.31 \mu_B$, which is close to the expected value from the Hund's rules. The crystalline and band structures were calculated by using the Density Functional Theory. Structural results obtained by considering a rhombohedral perovskite belonging to the $R\bar{3}$ space group are 98% in accordance with the experimental values. Close to the Fermi level, the band structure evidences strongly tendency to a half-metallicity behavior with semiconductor feature for the down spin orientation and conductor for the other. The mean value of the band gap is slightly smaller than the experimental value because the theoretical calculation was performed for the fundamental state, $T=0$ K, while the experimental measurement was performed at room temperature. The theoretical effective magnetic moment calculated from DFT, which is majority due to the Yb^{3+} isolated cation, is obtained to be $5.0 \mu_B$.

Acknowledgements

This work was partially supported by Division of Investigations of the National University of Colombia.

References

- [1] L.T. Corredor, J. Roa-Rojas, D.A. Landínez Téllez, R. Beltrán, P. Pureur, F. Mesquita and J. Albino Aguiar, J. Appl. Phys. 113 (2013) 17E302/1-3
- [2] D.P. Llamasa, D.A. Landínez Téllez and J. Roa-Rojas, Physica B 404 (2009) 2726 (2009).
- [3] M. Baazaoui, S. Zemni, M. Boudard, H. Rahmouni, A. Gasmi, A. Selmi and M. Oumezzine, Int. J. Nanoelectronics and Materials. 3 (2010) 23
- [4] A.M. Glazer, Acta Crystallogr. B 28 (1972) 3384

- [5] A.M. Glazer, Acta Crystallogr. A 31 (1975) 756
- [6] P.M. Woodward, Acta Crystallogr. B 53 (1997) 32
- [7] C.J. Howard, B.J. Kennedy and P.M. Woodward, Acta Crystallogr. B 59 (2003) 463
- [8] M. Wakeshima, D. Harada and Y. Hinatsu, J. Alloys and Compd. 287 (1999) 130
- [9] M. Wakeshima, D. Harada, Y. Hinatsu and N. Masaki, J. Solid State Chem. 47 (1999) 618
- [10] M. Wakeshima, D. Harada and Y. Hinatsu, J. Mater. Chem. 10 (2000) 419
- [11] C.M. Bonilla, D.A. Landínez Téllez, J. Arbey Rodríguez, E. Vera López and J. Roa-Rojas, Phys. B 398 (2008) 208
- [12] A.C. Larson and R.B. von Dreele, General Structure Analysis System GSAS (Los Alamos National Laboratory Report LAUR 2000), pp. 86-748.
- [13] P. Blaha, K. Schwarz, G.K.H. Madsen, D. Kvasnicka and J. Luitz, WIEN2k, an Augmented Plane Wave + Local Orbitals Program for Calculating Crystal Properties (Techn. Universität Wien, Vienna, 2001) ISBN 3-9501031-1-2.
- [14] S. Kausar, S. Joshi and A. Srivastava, Int. J. Nanoelectronics and Materials. 7 (2014) 77
- [15] F. D. Murnaghan, Proc. Natl. Acad. Sci. USA 30 (1944) 244
- [16] M.W. Lufaso and P.M. Woodward, Acta Crystallogr. B 57 (2001) 725
- [17] W. Wondratschek, *International Tables for Crystallography* (2006), Vol. A, Chapter 8.3, pp. 732-740.
- [18] E. Parthé, L. Gelato, B. Chabot, M. Penzo, K. Cenzual, R. Gladyshevskii, TYPIX Standardized and crystal chemical characterization of inorganic structure types. In: Gmelein Handbook of Inorganic and Organometallic Chemistry, 8th ed. (Springer, Berlin, 1993).
- [19] C. Kittel, *Introduction to Solid State Physics*, 6th Ed., John Wiley & Sons, Inc., New York, (1997) pp. 482
- [20] M. Bonilla, D.A. Landínez Téllez, J.A. Rodríguez, J. Albino Aguiar and J. Roa-Rojas, J. of Magn. Mater. 320 (2008) e397
- [21] H. Einollahzadeh, R.S. Dariani and S.M. Fazeli, Solid State Commun. 229 (2016) 1
- [22] Y. Zhao and D. G. Truhlar, J. of Chem. Phys. 130 (2009) 074103/1-3
- [23] T. Higuchi, T. Tsukamoto, N. Sata, M. Ishigame, Y. Tezuka and S. Shin, Phys. Rev. B 57 (1998) 6978
- [24] N. Kulagin, J. Dojcilovic and D. Popovic, Cryogenics 41 (2001) 745
- [25] Y. Zhao and D. G. Truhlar, J. Chem. Phys. 125 (2006) 194101/1-18
- [26] Y. Zhao and D. G. Truhlar, Acc. Chem. Res. 41 (2008) 157
- [27] E. Hosseine, Int. J. Nanoelectronics and Materials 8 (2015) 91